Model based concept to extract heart beat-to-beat variations beyond respiratory arrhythmia and baroreflex

Mindaugas Baranauskas[1*], Rytis Stanikūnas[2], Eugenijus Kaniušas[3], Arūnas Lukoševičius[1]

[1]Biomedical Engineering Institute, Kaunas University of Technology, Kaunas, Lithuania

[2]Institute of Psychology, Faculty of Philosophy, Vilnius University, Vilnius, Lithuania

[3]Institute of Biomedical Electronics, Vienna University of Technology, Vienna, Austria

*** Correspondence:**
Mindaugas Baranauskas
m.baranauskas@ktu.lt

Keywords: heart rate, beat-to-beat variations, neural regulation, modeling, personalization, respiratory arrhythmia, baroreflex, autonomic function

Abstract

The heart rate (HR) and its variability (HRV) reflect modulation of the autonomous nervous system, especially sympathovagal balance. The aim of this research was to develop a personalizable HR model and an in-silico system that could identify HR regulation parameters associated with respiratory arrhythmia (RSA) and baroreflex, and subsequently capture the residual heart beat-to-beat variations from individual psychophysiological recordings in humans. Here respiration signal, blood pressure signal and time instances of R peaks of EKG are used as input for the model. The model considers traditional lower-order mechanisms of HR dynamic, extracting residual displacements of the modeled R peaks relative to real R peaks. Three components – tonic, spontaneous and 0.1 Hz changes – can be seen in these R peak displacements. These dynamic residuals can help to analyze HRV beyond RSA and baroreflex, whereas our model-based concept suggests that the residuals are not merely modeling errors. The proposed method could help to investigate the presumably additional neural regulation impulses from higher-order brain and other influences.

1 Introduction

The heart rate (HR) regulation involves a number of hierarchical levels from the inner nervous system of the heart to cerebral cortex (Palma and Benarroch, 2014; Schmaußer et al., 2022). Respiratory sinus arrhythmia (RSA) and cardiac baroreflex – two main lower-order HR regulation mechanisms – can explain the majority of *HR variability (HRV)* (Draghici and Taylor, 2016), however they overshadow other interesting time-varying influences as HRV components. Besides, the respiration rate, age, sex and other factors need to be considered (or be controlled) for proper interpretation of HRV and for HRV comparison between individuals (Laborde et al., 2017; Shaffer and Ginsberg, 2017; Koenig et al., 2021).

Complex underlying regulation mechanisms and personal peculiarities are still not fully disclosed by traditional HRV measures, and other than traditional HRV measures are not always more helpful in clinical context though research on new ways to evaluate HR dynamics is still encouraged (Sassi et al., 2015)). *Alternative approach* would be to use statistical techniques to invert mathematically formulated forward models (Bach et al., 2018), or fitting HR dynamics to a comprehensive

personalizable HR regulation model to find weights of regulation mechanisms and analyze the residual HR dynamics unexplained by model.

Regulation at *lower levels* are more deterministic, more investigated and numerous heart-regulation models, tried to include this knowledge, for example models of Ursino (1998) and it's extensions (Ursino and Magosso, 2000; Hsing-Hua Fan and Khoo, 2002; Magosso et al., 2002; Cheng et al., 2010; Albanese et al., 2016; Park et al., 2020), Kotani et al (2005) and it's derivations (e.g. Ishbulatov et al., 2020), and other closed loop models (Van Roon et al., 2004; Ortiz-León et al., 2014) and specific purpose open loop models (Randall et al., 2019) for humans. Additional model linkage with registered biosignals would make the model adaptive and *personalizable*.

We also propose that HR variations unexplained by lower-order mechanisms (at least RSA and cardiac baroreflex) could be interpreted/used as an enhanced "signal/noise" ratio while seeking to capture other influences, e.g., associated with higher-order brain regulation mechanisms versus other influences. Activity in the higher brain areas has complex interactions, outcomes of activity in some higher-order brain structures has associations with specific autonomous nervous system (ANS) branches, e.g. parasympathetic influence could come from ventromedial prefrontal cortex (Wong et al., 2007; Ziegler et al., 2009; Schmaußer et al., 2022), right (Coote, 2013) or/and anterior (Chouchou et al., 2019) insular cortex, and sympathetic influence could come from left (Oppenheimer et al., 1992; Coote, 2013) or/and posterior (Chouchou et al., 2019) insular cortex, locus coeruleus (Mather et al., 2017). The effect of single parasympathetic impulse on HR is very fast and could vanish within one second (Spear et al., 1979; Berger et al., 1989), thus HR modeling preferably should be done with cardiac cycle to align parasympathetic bursts. However, known personalization solutions (Olufsen and Ottesen, 2013; Randall et al., 2019) use mean arterial blood pressure (ABP) – not continuous ABP signal with changes within inter-beat period. More granular timing could also help to extract higher-order HR regulation since brain stimulation correlates with HRV measures sensitive to fast changes in HR, e.g. high-frequency power (Schmaußer et al., 2022), however standard HRV measures usually generalize several minutes of psychophysiological data (Shaffer and Ginsberg, 2017). According to our knowledge, there is still no computational psychophysiologically based personalizable model of the HR regulation that considers ANS activity fluctuations within the cardiac cycle.

The *aim* of our article – to develop a computational model-based method that could identify heart rate regulation parameters associated with respiratory arrhythmia and baroreflex, and subsequently capture the remaining heart beat-to-beat variations from individual empirical human psychophysiological recordings.

First of all, the comprehensive computational HR lower-order neural control model for RSA and baroreflex is constructed. Subsequentially, a system for personalization of the model parameters by the use of experimental signals is presented. Results showing the residual HR variations beyond RSA and baroreflex possibly attributable to the higher-order brain control are shown and discussed.

2 Methods

HR regulation model encompasses three main domains: 1) heart, 2) brain – lower- and higher order neural control, and 3) vasculature (see **Figure 1**). The respiratory system could be interpreted as a lower-order neural control sub-domain if considered as a neural respiration center (due to link to NAmb). General scheme of main HRV mechanisms – RSA (*Respiration* center, *nucleus ambiguus* (NAmb), X cranial nervus vagus, sinoatrial node (SAN)) and baroreflexes (baroreceptors, *nucleus tractus solitarius* (NTS), NAmb for vagal effects; baroreceptors, NTS, rostral ventrolateral medulla (RVLM), intermediolateral column (IML) for sympathetic effects) – are inspired by Feher (2017,

This is a provisional file, not the final typeset article

613, his Figure 5.13.6) and Jänig (2006, 401). Most modules of this general scheme have a more detailed internal algorithmic structure described in dedicated parts of chapter 2.1. The respiration signal, ABP signal and time instances of the real R peaks of EKG are used as input for the model. HR model outputs the modeled R peaks and sympathetic nerve activity (SNA). HR model itself implements the alignment of the real and modeled R peaks needed for the later extraction of the residual HR variations – the displacements of the modeled R peaks relative to real R peaks – outside the model.

For empirical psychophysiological data fitting to the HR regulation model, the processed psychophysiological signals (procedure described in chapter 2.3.2) and manually configured set of various parameters (e.g., lower and upper boundaries of HR regulation model parameters) are passed to optimization algorithms (see left side of **Figure 2**) to find out set of beat-to-beat HR regulation model parameters with minimal error score. The error score calculation is based on the R peak displacements in time and SNA. The system for personalization of the model parameters is described in chapter 2.2.

The model is implemented in MATLAB Simulink environment and runs with ODE3 (Bogacki-Shampine) solver and fixed step of 1 milisecond.

2.1 Heart rate (HR) regulation model

2.1.1 Heart: Sinoatrial node – parasympathetic and sympathetic activity integration

The pharmacologicaly blocked or denervated during transplantation HR generated at SAN is practically constant for person (Jose and Collison, 1970; Zeuzem et al., 1991), however it slowly decreases with age (Jose and Collison, 1970). In our HR regulation model this *pacemaker* frequency is included as *HRbasal* variable (see **Figure 3**). If age is known, *HRbasal* can be defined by Jose and Collison (1970) formula:

$$\boldsymbol{HRbasal} = (\mathbf{118.1} - \mathbf{0.57} \times \boldsymbol{age}) \pm \mathbf{8}$$

Thus, for model parameters optimization we allow deviation up to 8 bmp from this computed value.

The SAN is innervated by the X cranial (vagus) nerve providing *parasympathetic input* and IML of the spinal cord providing *sympathetic input* (Palma and Benarroch, 2014) (see **Figure 1**, **Figure 3** to see its place in our model). Parasympathetic burst decelerates the HR with delay of about 0.2 s, the strongest effect is at approximately 0.5 s after the stimulation and vanishes after 1 s; meanwhile sympathetic burst accelerates the HR with delay of about 1-2 s (we set 1.5 s), the strongest effect is at approximately 4 s and vanishes at 20 s after the stimulation. We use custom made transfer function based on Spear (1979, their Figure 2) and Berger et al (1989, their Fig 4) empirical data for parasympathetic (see **Figure 4**) and sympathetic (see **Figure 5**) neural burst effect on heart period. Unlike Ursino (1998) and similar models where single first-order transfer function suggest exponential-like autonomic nervous system effect on heart period, here we use difference of two transfer functions to achieve gradual effect before its peak. In our SAN block, we use R-R intervals (RRI) rather than HR, because parasympathetic and sympathetic activity (bursts frequency) influence on RRI is almost linear (Draghici and Taylor, 2016; Geus et al., 2019).

The time-varying threshold for RRI is obtained by summing the heart period of denervated heart (60/*HRbasal*) and above-mentioned parasympathetic and sympathetic effects (see **Figure 3**). When the accumulated time after the last R peak is more than 300 ms and hits the dynamically changing RRI threshold, the pacemaker fires (a new R peak is generated) and is immediately reset to zero in

the "EKG R peak generation" sub-block (see **Figure 3** and **Figure 6**). Here time instances of modeled R peaks are stored in memory for analysis outside the model.

The key part in this HR model is sub-block for R alignment of the real and modeled R peaks (see **Figure 6** for its context within SAN sub-block, and **Figure 7** for its detailed implementation in Simulink). Usually, this block returns time instance of the previous real R peak as output for the corresponding modeled R peak; however, if the modeled R peak precedes the real R peak then infinity will be temporarily returned as "usable time of last R peak" – new modeled R peaks will be blocked – till reset by the next real R peak; if the real R peak preceded the modeled R peak, then update of output value will be blocked till new modeled R peak. This allows to model R peaks relative to time instances of the real R peaks. Besides, this approach enables to extract the R displacements by comparing real and the modeled EKG R peaks outside the model. However, this sub-block cannot deal with cases when the modeled R peak happens later than one real R peak; the additional re-check and correction of these cases outside the model is described in chapter 2.2.

2.1.2 Vasculature: Baroreception

Blood pulse wave stretches the vessel walls and reach arterial baroreceptors in the aortic arch and carotid sinus after 10-15 ms and 40-65 ms respectively, i.e., about 90 ms and 140 ms after R peak in EKG respectively (Edwards et al., 2009; Wehrwein and Joyner, 2013; Martins et al., 2014). Stimulation of aortic and carotid baroreceptors may have different impacts on HR control (Ishii et al., 2015), however we don't differentiate between them. We model the integrated baroreceptor activity and set an average 30 ms delay (see **Figure 8**). Some baroreceptors relatively more react to phasic changes to ABP, while some others more react to absolute level of ABP. Thus, for integration we add the derivative of ABP by coefficient *Pk* and scale resulting sum by *Kb*. Baroreceptors may take about 20 ms react to ABP (Borst and Karemaker, 1983) and the integrated baroreceptor activity peak is estimated at about 250 ms and extinguish till 390 ms after the EKG R (Edwards et al., 2009), thus, to match this with experimental or simulated data, we add 50 ms time lag for modified ABP signal *P* in our model. Baroreceptors (regardless of their place) has different activation thresholds, response functions and saturation levels (Wehrwein and Joyner, 2013; Feher, 2017, 610), thus, to generate within cardiac cycle varying baroafferent activity (*baro*), we use sigmoidal function which is similar to the used in Ursino (1998) model:

$$\boldsymbol{baro} = \frac{\boldsymbol{Bmax} \cdot \boldsymbol{e}^{\frac{\boldsymbol{P-Peq}}{\boldsymbol{Kab}}}}{\boldsymbol{1} + \boldsymbol{e}^{\frac{\boldsymbol{P-Peq}}{\boldsymbol{Kab}}}}$$

where *Peq* is the central point of the sigmoidal functional, *Kab* – slope-related coefficient, *Bmax* – saturation level (could be sensitive to postural position). Unlike Ursino (1998), we didn't set a minimal activation level since most baroreceptors don't show spontaneous activity and instead, we set tonic parasympathetic activity coming from higher-order brain to NTS (see **Figure 1**). Baroreception parameters values are suggested to be selected so that baroreceptors would be more sensitive to main pulse front and less sensitive to dicrotic notch.

2.1.3 Brain

2.1.3.1 Path via NTS for cardiac vagal and sympathetic baroreflexes

Baroreceptive information from the carotid and aortic baroreceptors travels via cranial nerves – glossopharyngeal and vagus respectively – and reaches the NTS in 10-15 ms (Wehrwein and Joyner, 2013; Martins et al., 2014). The NTS is the first central relay station of visceral afferent information

This is a provisional file, not the final typeset article

and is part of circuit for all medullary reflexes, including the baroreflex (Palma and Benarroch, 2014). NTS projects within 100–150 ms to areas responsible for baroreflex effects, including NAmb and RVLM, i.e. at about 200–300 ms after R peak in EKG (Edwards et al., 2001). Thus, we add 15 and 125 ms time delays correspondingly as the fixed values in the NTS scheme (see **Figure 9**).

NTS is under powerful control of the brain, integrates afferent information, and sends projections back almost to same great variety of neural structures, including brainstem, amygdala and (via thalamus) insular and prefrontal cortices (Jänig, 2006, 311–317). In this HR model, the NTS is set not to have spontaneous activity and to receive the integrated parasympathetic excitatory input *Sparas* from the "brain" (see **Figure 1** and **Figure 9**), and NTS is also the only structure receiving such input.

Baroreflex acts via NTS in three ways: as cardiac vagal (parasympathetic) baroreflex (via NAmb, see 2.1.3.2 subchapter), cardiac sympathetic baroreflex (via RVLM, see 2.1.3.3 subchapter) and non-cardiac sympathetic baroreflex (not relevant to our HR model). In cardiac vagal baroreflex circuit, NTS directly excites preganglionic cardiac vagal neurons in NAmb resulting in HR deceleration (Wehrwein and Joyner, 2013; Palma and Benarroch, 2014).

2.1.3.2 Preganglionic cardiac vagal neurons in nucleus ambiguus (NAmb) and Respiratory sinus arrhythmia (RSA)

The majority (about 80%) of preganglionic cardiac neurons originate from NAmb, effectively decelerate the HR via myelinated fibers, and their activity usually is mostly similar to respiration pattern (Coote, 2013); effect of other cardiac vagal neurons is relatively small, more delayed and slower than those of NAmb (Coote, 2013). The NAmb neurons are not active spontaneously themselves – they are excited by other brainstem areas, predominantly by the NTS, and are inhibited by medullary ventral respiratory group neurons ('respiration center') only during inspiration, i.e. are not blocked during expiration or breath holding, apnea (Dergacheva et al., 2010; Palma and Benarroch, 2014; Feher, 2017, 612–613), though this inhibition is not complete and does not imply absence of inhibition later (Geus et al., 2019). The aggregated effect causes RSA – temporal withdrawal of predominant parasympathetic activity causing the acceleration of the HR during inspiration. Thus, we include only preganglionic cardiac neurons of NAmb with excitatory input from NTS (incorporating baroreceptive information) and inhibition by multiplication of square root of respiration signal derivative and transfer function with *Krsa* and *Drsa* parameters only at inspiration (see **Figure 10**). NAmb output activity is set to be always non-negative.

2.1.3.3 Rostral ventrolateral medulla (RVLM) for sympathetic baroreflex

The aggregated effect of baroreceptor stimulation inhibits sympathetic activity. In sympathetic baroreflex circuit, NTS via caudal ventrolateral medulla (CVLM) or directly inhibits RVLM (Wehrwein and Joyner, 2013; Palma and Benarroch, 2014). Thus, in our model's overview scheme NTS is shown to act on "(R)VLM" (see **Figure 1**).

Sympathetic baroreflex does not produce sympathetic outflow by itself: if central sympathetic activity would be low or insufficient (e.g., during anesthesia), sympathetic baroreflex will not be noticeable (Karemaker, 2022). RVLM has spontaneous activity itself and receives various excitatory inputs (Jänig, 2006, 393–396). Sympathoexcitatory RVLM neurons are activated by psychological stress, pain, hypoxia, hypovolemia, and hypoglycemia both directly and via descending inputs from the higher order structures (e.g., insula, prefrontal cortex, amygdala, and hypothalamic subnuclei) (Palma and Benarroch, 2014; Barman and Yates, 2017). In this HR model, the RVLM theoretically has constant spontaneous activity *Arvlm_sp* and receives the integrated sympathetic excitatory input

from "brain" *Ssmpt* (see left side of **Figure 11** and sub-chapter 2.1.3.4 below) – RVLM is also the only structure receiving such input.

RVLM output has a pulsatile pattern, and it is seen when it is not blocked by NTS/CVLM. The inhibiting NTS/CVLM activity itself seems to be too short to achieve only short RVLM impulses when tonic NTS/CVLM level drops. How exactly this happens in ventrolateral medulla is not known, thus we implement two first-order transfer functions to obtain a closer-to-desired effect, only one of these transfer functions has variable parameters (*Kcvlm* and *Dcvlm*) and is just conventionally named as CVLM (see **Figure 11**).

Just started model would produce long-term lasting strong sympathetic effects on heart rate and vasculature, thus we temporarily turn off RVLM for 5 seconds till parasympathetic activity via NTS/CVLM would regularly inhibit RVLM and limit RVLM output to saturation value *Arvlm_mx* (see right side of **Figure 11**).

The SNA generated by RVLM travels via sympathetic IML of the spinal cord; IML neurons serve as a common sympathetic effector and via sympathetic ganglia innervate the blood vessels (non-cardiac (arterial) sympathetic baroreflex, which is not relevant to our HR model) and the heart (cardiac sympathetic baroreflex) (Wehrwein and Joyner, 2013; Palma and Benarroch, 2014). Cardiac sympathetic baroreflex effect on withdrawal of sympathetic HR acceleration described in chapter 2.1.1).

2.1.3.4 Higher-order regulation

The intrinsic HR is about 40 bmp faster than resting state mean HR due to dominance of parasympathetic influence (Smetana and Malik, 2013) and higher-order brain regulation is critical to maintain it, e.g., by salience network (were anterior insular and anterior cingulate cortices are core of it) (Guo et al., 2016) and (pre-)frontal cortex (Wong et al., 2007; Thayer and Lane, 2009; Ziegler et al., 2009; Smith et al., 2017). Mere thickness of prefrontal cortex and insula positively correlates with the resting HRV (Koenig et al., 2021). In our model, this higher-order parasympathetic activity is included as *Sparas* parameter (see **Figure 1**).

Theoretically, tonic sympathetic activity could be set as *Ssmpt* parameter (see **Figure 1**), however during parameter optimization we cannot differentiate *Arvlm_sp* and *Ssmpt*, thus we practically set *Ssmpt* = 0 and *Arvlm_sp* means constant sum of RVLM spontaneous activity and sympathetic excitatory input from "brain" (see **Figure 11** and sub-chapter 2.1.3.3 above).

2.2 System for model personalization

Although HR regulation model usually returns the correctly aligned real and modeled R peaks, re-check and correction is needed for rare cases of the skipped modeled R peak: if the real n^{th} R peak was earlier than $(n–1)^{th}$ modeled R peak, then *NaN (not a number)* must be inserted for the skipped modeled R peak (see right side of **Figure 2**).

Based on the displacements of the modeled R peaks relative to the real R peaks and SNA, the error score is calculated. Error score is used for its minimization during parameters optimization and is calculated only for period starting from 30 seconds after the beginning of simulation. Error score is sum of two components listed below (see also right side of **Figure 2**):

1. *root mean square (RMS) of R peaks displacements* (i.e., RMS of time instance differences between the real R peaks and the corresponding aligned modeled R peaks) in milliseconds;
2. *penalty score* which consists of:

This is a provisional file, not the final typeset article

- penalty of 200 × the ratio of the skipped modeled R peaks and all real R peaks within analysis period; such penalty is added only if this ratio > 5%;
- penalty due to the modeled integrated SNA properties by summing (up to maximum sum of 250):
  - penalty of 50 – if any SNA lower peak is higher peak > 0;
  - penalty of 50 – if SNA saturates for longer than 0.3 s period uninterruptedly;
  - penalty of 50 – if ratio of unique SNA values and number of all real R peaks within analysis period < 10%;
  - penalty of 100 × (SNA peak relative to R peak as found by cross-correlation – 0.8) – only if SNA peaks are more than 0.8 s after R peaks;
  - penalty of 200 – if SNA is zero all the time.

Since optimization algorithms hardly can find global minimum, and the lowest local minimum may not be psychophysiologically meaningful by parameters combination (as a whole, or due to stuck at floors or ceils of boundaries) or by morphology of the modeled R peaks sequence, several invocations of these optimization algorithms may be needed to find out the most acceptable local minimum (see left side of **Figure 2**). Thus, the best optimized solutions must be manually reviewed.

For personalization of HR model parameters, the selected initial bounds of parameters are provided in **Table 1**. In total, 15(-16) model parameters could be personalized (16th *Ssmpt* is theoretical, practically not used). Lower and upper boundaries or initial values for several of them could be roughly estimated by physiological norms (e.g., *HRbasal* by knowing age) or from other models having similar components (e.g., *Peq* and *Kab* from Ursino (1998) model); boundaries for remaining parameters suggested by our internal manual research (see **Table 1** for summary) to avoid often stuck at boundaries during parameters optimization and to avoid too often search in too broad range leading to the wrong optimization result, e.g., to avoid the modeled HR being constant at mean of the real HR.

Optimization of HR regulation model parameters is done with MATLAB *particleswarm* and *patternsearch* algorithms from Global Optimization Toolbox: former for initial random selection of model parameters, and later to find more precise solution with minimal error score. Successful optimization required to change *patternsearch* optimization algorithms parameters from the defaults: tolerance on the function ("FunctionTolerance") set to 0.001, i.e. to stop iterations if the change in function value is less than 0.001; tolerance on the variable ("StepTolerance") to stop iterations if both the change in position and the mesh size are less than 0.001; polling strategy used in the pattern search ("PollMethod") set to GSSPositiveBasis2N (which is similar to the default GPSPositiveBasis2N, but GSSPositiveBasis2N is more efficient than GPSPositiveBasis2N when the current point is near a linear constraint boundary); order of poll directions in pattern search ("PollOrderAlgorithm") changed to "Random"; complete poll around the current point ("UseCompletePoll") was enabled. The changed optimization algorithms parameter from the default for *particleswarm*: "FunctionTolerance" set to 0.001, i.e. to end iterations when the relative change in best objective function value over the last 20 iterations is less than 0.001. One invocation of the selected optimization algorithm runs the HR regulation model multiple times – each time with a different set of HR model parameters.

2.3 Testing of model-based concept

2.3.1 Participants, equipment and procedure

Two male healthy participants (aged 33 and 50, without any heart-related problems) volunteered in the pilot recordings to fit our HR model. These pilot recordings were conducted following the ethical

principles of the Declaration of Helsinki, including written informed consent and voluntary participation.

Psychophysiological recordings were performed with BIOPAC MP150 (Biopac Systems Inc., 42 Aero Camino, Goleta, CA, United States) with ECG electrodes placed according to lead II and the respiration belt on abdomen. ABP was registered with Portapres device (Finapres Medical Systems BV, Palatijn 3, Enschede, Netherlands) using finger cuffs.

Participants were in supine position for 10 min rest, followed by 3 min slow breathing and again 10 min rest.

2.3.2 Offline signal processing

The *EKG* signal was 0.4–35 Hz band-pass filtered offline using Butterworth filter. Time instances of EKG R peaks were identified from EKG signal using modified Pan-Tompkins (1985) algorithm and additionally visually inspected together with raw EKG signal. Wrongly detected R peaks were manually corrected by selecting the real EKG R time as signal peak or were interpolated.

Respiration signal was low-pass filtered with cut-off at 0.4 Hz and normalized between –0.5 and 0.5.

Since *ABP* registered at hand's fingers, ABP signal was shifted by –100 ms to compensate blood arrival time difference between baroreceptors and fingers. ABP signal was low-pass filtered with cut-off at 10 Hz. Baseline was changed to 80 mmHg.

2.3.3 Derived psychophysiological data

The additional psychophysiological data were derived for more comprehensive visualization of results. To see RSA-mediated HR variations together with respiration signal, the real HR was directly derived from time instances of the R peaks. Meanwhile virtual HR was derived from difference between the real RRI and the corresponding R peak displacements (not by using RRI from the modeled R peaks). To see ABP associations with baroreflex-mediated SNA and HR variations, the systolic and diastolic blood pressure were derived as upper and lower envelopes of the processed ABP signal correspondingly. The standard deviation of RRI (SDNN) for entire 23 min record was computed to evaluate general HRV.

2.3.4 Additional details regarding psychophysiological data fitting to model

For parameters personalization, the HR model has been run across the entire 23 minutes length of empirical psychophysiological records on MATLAB R2022b parallel pool of 45 processes in a computer with AMD Ryzen Threadripper PRO 5995WX 64-Cores 2.70 GHz processor, 128 GB RAM.

3 Results

The processed experimental psychophysiological data was fitted to the HR regulation model by evaluating multiple sets of parameters to find out solution with minimal error score, i.e., sum of minimal RMS of R peak displacements and penalty score.

Optimization of HR model parameters was called twice with *particleswarm* algorithm and once with *patternsearch* algorithm – after each invocation passing the best solution for next optimization as initial set. For parameters personalization of a 33 years old male, in total 11859 evaluations of model parameter's sets in Simulink took about 3 hours and 11 minutes to obtain the most optimal solution with RMS of R peak displacements 49.051 ms for time period from 30 s to 23 minute (SDNN of real

This is a provisional file, not the final typeset article

RRI was 88.263); for a 50 years old male – 17533 evaluations took about 4 hours and 43 minutes and resulted in optimal solution with RMS of R peak displacements 27.925 ms (SDNN of real RRI was 32.038). In both cases, the most optimal solutions had no penalty score. See **Table 1** for list of the most optimal sets of personalized parameters.

The main result of our proposed concept is the time course of R peak displacements (see C and F parts of **Figure 12** and **Figure 13** for 33- and 50-year-old males correspondingly). R peak displacements of 33-years-old male had relatively stable baseline despite the real HR baseline drifts (see **Figure 12**A), even during shifts between resting and slow breathing periods. R peak displacements had pulsations of about 0.1 Hz at multiple time intervals (see **Figure 12**F) that often resemble ABP (see **Figure 12**E) with time delay of about 2.2 s. Besides, some R peak displacements overshot the mentioned pulsations just for single RRI and these momentary heart decelerations were up to 280 ms compared to the expected by the personalized HR model (marked with red arrows in **Figure 12**F, e.g., the largest one appeared at 82 second). These decelerations often occurred at rising part of slow R peak displacement pulsations after previous drop of ABP with SNA burst (see **Figure 12**E) and expiration (see **Figure 12**D). Indeed, in both 33- and 50-year-old male cases, SNA is more often and more strongly generated at drops in ABP via withdrawal of the modeled baroafferent activity (this is more clearly seen in **Figure 12**E). Meanwhile, the baseline drifts existed in R peak displacements of 50-years-old male (**Figure 13**C). Here R peak displacements did not resemble ABP in general, though few morphological similarities also could be envisioned, e.g., about 0.1 Hz pulsations at about 970–990 second and baseline drop at about 1060–1090 seconds intervals (compare **Figure 13** parts E and F). In both cases the time course of R peak displacements was dissimilar to respiration, and especially in 50-year-old male case the fast virtual HR variations mimicked the respiration and the corresponding real HR patterns (see D parts of **Figure 12** and **Figure 13**). Thus, three main components of R peak displacements may be visible to different individuals even during the same resting condition: very slow baseline drifts (<0.1 Hz), about 0.1 Hz pulsations, momentary fast irregularities.

4 Discussion

The concept of computerized physiology modeling followed in the article is based on the integration of basic physiology knowledge and cutting-edge computing technologies into virtual models. Virtual models allow not only to more effectively investigate physiological mechanisms, predict multiple influences, but also apply modeling results to biosignal and data processing, research and clinical decision making (Pruett et al., 2020). This is especially relevant to the progress of personal medicine, prediction, and prevention. Modeling of HR regulation is an essential part of such approaches as virtual physiological human (www.vph-institute.org), or virtual patients for *in silico* trials (Sinisi et al., 2021). Article contributes for two main research problems in modeling of HR regulation: 1) how to integrate the abundant knowledge of physiology, psychology and biophysics in the form of formal models that are easily accessible to the user of computerized systems; and 2) how to enrich these models with additional empirical personal data, thereby refining the models and personalizing the decisions they could support.

The specific purpose of this paper was to present concept of a computational method that could identify personalizable HR regulation parameters and capture the beat-by-beat variations (R peak displacements) that are expected not to be attributable to lower order HR regulation mechanisms – respiratory arrhythmia and cardiac baroreflex. To our knowledge, such a method incorporating multilevel model of HR regulation, designed to be fitted to empirical data, and seeking to extract residual HR irregularities, has not yet been proposed. A valuable feature of the model is a

presentation of neurophysiological regulatory mechanisms in visual form of SIMULINK block diagrams, making the model and simulation easily interactive and interpretable.

In comparison – most of the available models allow modeling of generalized humans without availability to fit the model to the concrete person. There are also attempts to create patient specific models (Gray and Pathmanathan, 2018) and the trend is to create more universal models suitable for either normal or pathological – personalized – conditions paving the path from the virtual physiological human to the clinic (Hoekstra et al., 2018). One of popular models in MATLAB SIMULINK environment – PNEUMA (Hsing-Hua Fan and Khoo, 2002; Cheng et al., 2010) although is highly elaborated, can simulate multiple influences even within heart period, however it is too complex and would be too slow for search of parameters combinations for beat-to-beat personalization. Some newer models relying on the knowledge of lower-level mechanisms, propose more elaborated neural regulations at relatively higher levels; for example, Park et al. (2020) model included more detailed parasympathetic activity regulation via NTS, NAmb and dorsal motor nucleus of the vagus – but this is still about regulation at lower-order medulla oblongata level. Although HR regulation models involving multiple higher brain structures have already been described in the literature (Thayer and Lane, 2009; e.g. Smith et al., 2017), but they lack time axis and mathematical formulations.

To evaluate HR regulation influences, particularly those attributable to higher-order regulations, a model of lower-order regulations should be adequate to the *in vivo* HRV. Particularly our proposed model was able to simulate RSA and cardiac baroreflex mimicking morphology of the real HR. Our model personalization system was able to find parameter sets of HR model for two males encompassing two psychophysiological conditions – resting and slow breathing. Both different sets were useful to generate R peak displacements that are dissimilar to respiration morphology, suggesting that architecture of RSA mechanism is adequate in our HR model.

Our proposed concept reveals the possibility to separate three components of R peak displacements and analyze them separately: tonic, spontaneous and 0.1 Hz changes. The *tonic component*, like baseline drifts seen in 50 years old male case, could be associated to mental, physiological, humoral state slow changes. The *spontaneous changes* in the R peak displacements are seen in the 33 years old male recording, while preliminary, suggests that there are possibly other factors here, perhaps sudden sporadically changed parasympathetic activity from higher-order areas of the brain, maybe partly due to additional interaction between baroinformation and RSA. The *0.1 Hz component* possibly related to Mayer waves, insufficient model adequacy in simulating the baroreflex from ABP. There is 2.2 seconds delay of R displacements relative to ABP (see **Figure 12** E and F parts) and it cannot be fitted to faster vagal or slower sympathetic baroreflex mechanisms – therefore the existing model could be improved by adding new mechanisms, their interactions or additional input could be implemented. Nevertheless, interesting insights can come by analyzing components of R peak displacements extracted by our concept even as it is without modifications.

Our proposed model-based computational method has limitations and simplifications worth noting which may be improved in future. One limitation is assuming the constant tonic ANS activity level as higher-order neural control, though an effective input from higher-order brain is expected at about 400–600 ms after EKG R as suggested from our previous study (Baranauskas et al., 2021). Also, our model currently does not simulate orthostatic hypotension, thus this model is intended to be used when the person remains in the same posture. Furthermore, in our proposed approach, unexplained HR variations are provisionally attributed to higher-order brain regulation, however it could be attributed to any heart regulation level. Anyway, we believe this approach could help to investigate brain-heart interactions by enhancing ratio between influences from brain and other HR regulation mechanisms. Future studies could try to discriminate sources of R peaks displacements (e.g., higher-

This is a provisional file, not the final typeset article

order neural or humoral; sympathetic or parasympathetic). Model-based computational system should be tested on broader sample of subjects to reflect sex, age and specific illnesses; for example, it is known that cardiac vagal baroreflex is relatively more pronounced in females and sympathetic baroreflex in males (Kim et al., 2011).

The model-based concept could be further applied to *in-silico* analysis of heart regulation in health care, medical diagnostics, psychology, and research of the heart-brain interactions. The model parameters themselves could be useful for the assessment of the respiratory arrhythmia and the baroreflex. R displacements could help to control RSA and/or baroreflex effects in stress, fatigue, emotion studies or biofeedback systems while assessing tonic, phasic and/or spontaneous changes in HR. Model could help to develop diagnostic and screening biomarkers (e.g., sympathovagal balance) based on HRV data retrieved from wearable devices. The developed computational system integrating the psychophysiological mechanisms of HR regulation in the form of a formalized personalized model may facilitate further research and reveal new features of HR regulation that would be useful in practice.

Data Availability Statement

The computational system implementing this model-based concept can be downloaded from open source Zenodo repository: <https://doi.org/10.5281/zenodo.7765459>. The raw psychophysiological data supporting the conclusions of this article will be made available by the authors, without undue reservation.

Ethics statement

Pilot recordings are used as the basis for the ethic application (namely, for the estimation of the effect size and thus for the necessary size of the clinical study). These pilot recordings were conducted following the ethical principles of the Declaration of Helsinki, including written informed consent and voluntary participation.

Conflict of Interest

The authors declare that the research was conducted in the absence of any commercial or financial relationships that could be construed as a potential conflict of interest.

Author Contributions

MB and RS contributed to conception. AL and MB contributed to funding acquisition. EK designed the pilot study for data collection. EK and MB did pilot study and collected the data. MB cared about modeling, software, data analysis, interpretation, visualization of results, and wrote the first draft of the manuscript. All authors contributed to manuscript revision, read, and approved the submitted version.

Funding

This work was funded by the European Social Fund under No 09.3.3-LMT-K-712 “Development of Competences of Scientists, other Researchers and Students through Practical Research Activities” measure.

Acknowledgments

We thank Vienna University of Technology Institute of Biomedical Electronics for laboratory equipment for psychophysiological recordings. We thank Lena Kummer for her assistance in the experimental study. We thank all the volunteers for their participation in the study.

References

Albanese, A., Cheng, L., Ursino, M., and Chbat, N. W. (2016). An integrated mathematical model of the human cardiopulmonary system: model development. *Am. J. Physiol.-HEART Circ. Physiol.* 310, H899–H921. doi: 10.1152/ajpheart.00230.2014.

Bach, D. R., Castegnetti, G., Korn, C. W., Gerster, S., Melinscak, F., and Moser, T. (2018). Psychophysiological modeling: Current state and future directions. *Psychophysiology* 55, e13214. doi: 10.1111/psyp.13209.

Baranauskas, M., Grabauskaitė, A., Griškova-Bulanova, I., Lataitytė-Šimkevičienė, B., and Stanikūnas, R. (2021). Heartbeat evoked potentials (HEP) capture brain activity affecting subsequent heartbeat. *Biomed. Signal Process. Control* 68, 102731. doi: 10.1016/j.bspc.2021.102731.

Barman, S. M., and Yates, B. J. (2017). Deciphering the Neural Control of Sympathetic Nerve Activity: Status Report and Directions for Future Research. *Front. Neurosci.* 11. doi: 10.3389/fnins.2017.00730.

Berger, R. D., Saul, J. P., and Cohen, R. J. (1989). Transfer function analysis of autonomic regulation. I. Canine atrial rate response. *Am. J. Physiol. - Heart Circ. Physiol.* 256, H142–H152.

Borst, C., and Karemaker, J. M. (1983). Time delays in the human baroreceptor reflex. *J. Auton. Nerv. Syst.* 9, 399–409. doi: 10.1016/0165-1838(83)90004-8.

Cheng, L., Ivanova, O., Fan, H.-H., and Khoo, M. C. K. (2010). An integrative model of respiratory and cardiovascular control in sleep-disordered breathing. *Respir. Physiol. Neurobiol.* 174, 4–28. doi: 10.1016/j.resp.2010.06.001.

Chouchou, F., Mauguière, F., Vallayer, O., Catenoix, H., Isnard, J., Montavont, A., et al. (2019). How the insula speaks to the heart: Cardiac responses to insular stimulation in humans. *Hum. Brain Mapp.* 40, 2611–2622. doi: 10.1002/hbm.24548.

Coote, J. H. (2013). Myths and realities of the cardiac vagus. *J. Physiol.* 591, 4073–4085. doi: 10.1113/jphysiol.2013.257758.

Dergacheva, O., Griffioen, K. J., Neff, R. A., and Mendelowitz, D. (2010). Respiratory modulation of premotor cardiac vagal neurons in the brainstem. *Respir. Physiol. Neurobiol.* 174, 102–110. doi: 10.1016/j.resp.2010.05.005.

Draghici, A. E., and Taylor, J. A. (2016). The physiological basis and measurement of heart rate variability in humans. *J. Physiol. Anthropol.* 35, 22. doi: 10.1186/s40101-016-0113-7.

This is a provisional file, not the final typeset article

Edwards, L., Ring, C., McIntyre, D., and Carroll, D. (2001). Modulation of the human nociceptive flexion reflex across the cardiac cycle. *Psychophysiology* 38, 712–718. doi: 10.1111/1469-8986.3840712.

Edwards, L., Ring, C., McIntyre, D., Winer, J. B., and Martin, U. (2009). Sensory detection thresholds are modulated across the cardiac cycle: Evidence that cutaneous sensibility is greatest for systolic stimulation. *Psychophysiology* 46, 252–256. doi: 10.1111/j.1469-8986.2008.00769.x.

Feher, J. (2017). *Quantitative Human Physiology*. 2nd ed. Boston: Academic Press Available at: https://www.sciencedirect.com/science/article/pii/B9780128008836000951.

Geus, E. J. C. de, Gianaros, P. J., Brindle, R. C., Jennings, J. R., and Berntson, G. G. (2019). Should heart rate variability be "corrected" for heart rate? Biological, quantitative, and interpretive considerations. *Psychophysiology* 56, e13287. doi: https://doi.org/10.1111/psyp.13287.

Gray, R. A., and Pathmanathan, P. (2018). Patient-Specific Cardiovascular Computational Modeling: Diversity of Personalization and Challenges. *J Cardiovasc. Transl. Res.* 11, 80–88. doi: 10.1007/s12265-018-9792-2.

Guo, C. C., Sturm, V. E., Zhou, J., Gennatas, E. D., Trujillo, A. J., Hua, A. Y., et al. (2016). Dominant hemisphere lateralization of cortical parasympathetic control as revealed by frontotemporal dementia. *Proc. Natl. Acad. Sci.* 113, E2430–E2439. doi: 10.1073/pnas.1509184113.

Hoekstra, A. G., van Bavel, E., Siebes, M., Gijsen, F., and Geris, L. (2018). Virtual physiological human 2016: translating the virtual physiological human to the clinic. *Interface Focus* 8. doi: 10.1098/rsfs.2017.0067.

Hsing-Hua Fan, and Khoo, M. C. K. (2002). PNEUMA - a comprehensive cardiorespiratory model. in *Proceedings of the Second Joint 24th Annual Conference and the Annual Fall Meeting of the Biomedical Engineering Society] [Engineering in Medicine and Biology*, 1533–1534 vol.2. doi: 10.1109/IEMBS.2002.1106522.

Ishbulatov, Y. M., Karavaev, A. S., Kiselev, A. R., Simonyan, M. A., Prokhorov, M. D., Ponomarenko, V. I., et al. (2020). Mathematical modeling of the cardiovascular autonomic control in healthy subjects during a passive head-up tilt test. *Sci. Rep.* 10, 1–11. doi: 10.1038/s41598-020-71532-7.

Ishii, K., Mitsuhiro, I., and Matsukawa, K. (2015). Differential contribution of aortic and carotid sinus baroreflexes to control of heart rate and renal sympathetic nerve activity. *J. Physiol. Sci.* 65, 471–480. doi: 10.1007/s12576-015-0387-2.

Jänig, W. (2006). *Integrative Action of the Autonomic Nervous System: Neurobiology of Homeostasis*. Cambridge University Press.

Jose, A. D., and Collison, D. (1970). The normal range and determinants of the intrinsic heart rate in man. *Cardiovasc. Res.* 4, 160–167. doi: 10.1093/cvr/4.2.160.

Karemaker, J. M. (2022). The multibranched nerve: vagal function beyond heart rate variability. *Biol. Psychol.* 172, 108378. doi: 10.1016/j.biopsycho.2022.108378.

Kim, A., Deo, S. H., Vianna, L. C., Balanos, G. M., Hartwich, D., Fisher, J. P., et al. (2011). Sex differences in carotid baroreflex control of arterial blood pressure in humans: relative contribution of cardiac output and total vascular conductance. *Am. J. Physiol. - Heart Circ. Physiol.* 301, H2454–H2465. doi: 10.1152/ajpheart.00772.2011.

Koenig, J., Abler, B., Agartz, I., Åkerstedt, T., Andreassen, O. A., Anthony, M., et al. (2021). Cortical thickness and resting-state cardiac function across the lifespan: A cross-sectional pooled mega-analysis. *Psychophysiology* 58, e13688. doi: https://doi.org/10.1111/psyp.13688.

Kotani, K., Struzik, Z. R., Takamasu, K., Stanley, H. E., and Yamamoto, Y. (2005). Model for complex heart rate dynamics in health and diseases. *Phys. Rev. E* 72, 41904. doi: 10.1103/PhysRevE.72.041904.

Laborde, S., Mosley, E., and Thayer, J. F. (2017). Heart Rate Variability and Cardiac Vagal Tone in Psychophysiological Research – Recommendations for Experiment Planning, Data Analysis, and Data Reporting. *Front. Psychol.* 8. doi: 10.3389/fpsyg.2017.00213.

Magosso, E., Cavalcanti, S., and Ursino, M. (2002). Theoretical analysis of rest and exercise hemodynamics in patients with total cavopulmonary connection. *Am. J. Physiol.-Heart Circ. Physiol.* 282, H1018–H1034. doi: 10.1152/ajpheart.00231.2001.

Martins, A. Q., McIntyre, D., and Ring, C. (2014). Effects of baroreceptor stimulation on performance of the Sternberg short-term memory task: A cardiac cycle time study. *Biol. Psychol.* 103, 262–266. doi: 10.1016/j.biopsycho.2014.10.001.

Mather, M., Joo Yoo, H., Clewett, D. V., Lee, T.-H., Greening, S. G., Ponzio, A., et al. (2017). Higher locus coeruleus MRI contrast is associated with lower parasympathetic influence over heart rate variability. *NeuroImage* 150, 329–335. doi: 10.1016/j.neuroimage.2017.02.025.

Olufsen, M. S., and Ottesen, J. T. (2013). A practical approach to parameter estimation applied to model predicting heart rate regulation. *J. Math. Biol.* 67, 39–68. doi: 10.1007/s00285-012-0535-8.

Oppenheimer, S. M., Gelb, A., Girvin, J. P., and Hachinski, V. C. (1992). Cardiovascular effects of human insular cortex stimulation. *Neurology* 42, 1727–1732. doi: 10.1212/WNL.42.9.1727.

Ortiz-León, G., Vílchez-Monge, M., and Montero-Rodríguez, J. J. (2014). Simulations of the Cardiovascular System Using the Cardiovascular Simulation Toolbox. in *5th Workshop on Medical Cyber-Physical Systems* OpenAccess Series in Informatics (OASIcs)., eds. V. Turau, M. Kwiatkowska, R. Mangharam, and C. Weyer (Dagstuhl, Germany: Schloss Dagstuhl–Leibniz-Zentrum fuer Informatik), 28–37. doi: 10.4230/OASIcs.MCPS.2014.28.

Palma, J.-A., and Benarroch, E. E. (2014). Neural control of the heart: recent concepts and clinical correlations. *Neurology* 83, 261–271. doi: 10.1212/WNL.0000000000000605.

This is a provisional file, not the final typeset article

Pan, J., and Tompkins, W. J. (1985). A Real-Time QRS Detection Algorithm. *IEEE Trans. Biomed. Eng.* BME-32, 230–236. doi: 10.1109/TBME.1985.325532.

Park, J. H., Gorky, J., Ogunnaike, B., Vadigepalli, R., and Schwaber, J. S. (2020). Investigating the Effects of Brainstem Neuronal Adaptation on Cardiovascular Homeostasis. *Front. Neurosci.* 0. doi: 10.3389/fnins.2020.00470.

Pruett, W. A., Clemmer, J. S., and Hester, R. L. (2020). Physiological Modeling and Simulation—Validation, Credibility, and Application. *Annu. Rev. Biomed. Eng.* 22, 185–206. doi: 10.1146/annurev-bioeng-082219-051740.

Randall, E. B., Billeschou, A., Brinth, L. S., Mehlsen, J., and Olufsen, M. S. (2019). A model-based analysis of autonomic nervous function in response to the Valsalva maneuver. *J. Appl. Physiol.* 127, 1386–1402. doi: 10.1152/japplphysiol.00015.2019.

Sassi, R., Cerutti, S., Lombardi, F., Malik, M., Huikuri, H. V., Peng, C.-K., et al. (2015). Advances in heart rate variability signal analysis: joint position statement by the e-Cardiology ESC Working Group and the European Heart Rhythm Association co-endorsed by the Asia Pacific Heart Rhythm Society. *EP Eur.* 17, 1341–1353. doi: 10.1093/europace/euv015.

Schmaußer, M., Hoffmann, S., Raab, M., and Laborde, S. (2022). The effects of noninvasive brain stimulation on heart rate and heart rate variability: A systematic review and meta-analysis. *J. Neurosci. Res.* doi: 10.1002/jnr.25062.

Shaffer, F., and Ginsberg, J. P. (2017). An Overview of Heart Rate Variability Metrics and Norms. *Front. Public Health* 5. doi: 10.3389/fpubh.2017.00258.

Sinisi, S., Alimguzhin, V., Mancini, T., Tronci, E., and Leeners, B. (2021). Complete populations of virtual patients for in silico clinical trials. *Bioinformatics* 36, 5465–5472. doi: 10.1093/bioinformatics/btaa1026.

Smetana, P., and Malik, M. (2013). Sex differences in cardiac autonomic regulation and in repolarisation electrocardiography. *Pflüg. Arch. Eur. J. Physiol.* 465, 699–717. doi: 10.1007/s00424-013-1228-x.

Smith, R., Thayer, J. F., Khalsa, S. S., and Lane, R. D. (2017). The hierarchical basis of neurovisceral integration. *Neurosci. Biobehav. Rev.* 75, 274–296. doi: 10.1016/j.neubiorev.2017.02.003.

Spear, J. F., Kronhaus, K. D., Moore, E. N., and Kline, R. P. (1979). The effect of brief vagal stimulation on the isolated rabbit sinus node. *Circ. Res.* 44, 75–88. doi: 10.1161/01.RES.44.1.75.

Thayer, J. F., and Lane, R. D. (2009). Claude Bernard and the heart–brain connection: Further elaboration of a model of neurovisceral integration. *Neurosci. Biobehav. Rev.* 33, 81–88. doi: 10.1016/j.neubiorev.2008.08.004.

Ursino, M. (1998). Interaction between carotid baroregulation and the pulsating heart: a mathematical model. *Am. J. Physiol. - Heart Circ. Physiol.* 275, H1733–H1747.

Ursino, M., and Magosso, E. (2000). Acute cardiovascular response to isocapnic hypoxia. I. A mathematical model. *Am. J. Physiol.-Heart Circ. Physiol.* 279, H149–H165. doi: 10.1152/ajpheart.2000.279.1.H149.

Van Roon, A. M., Mulder, L. J. M., Althaus, M., and Mulder, G. (2004). Introducing a baroreflex model for studying cardiovascular effects of mental workload. *Psychophysiology* 41, 961–981. doi: 10.1111/j.1469-8986.2004.00251.x.

Wehrwein, E. A., and Joyner, M. J. (2013). "Chapter 8 - Regulation of blood pressure by the arterial baroreflex and autonomic nervous system," in *Handbook of Clinical Neurology* Autonomic Nervous System., ed. R. M. B. and D. F. Swaab (Elsevier), 89–102. Available at: http://www.sciencedirect.com/science/article/pii/B9780444534910000080 [Accessed April 22, 2016].

Wong, S. W., Massé, N., Kimmerly, D. S., Menon, R. S., and Shoemaker, J. K. (2007). Ventral medial prefrontal cortex and cardiovagal control in conscious humans. *NeuroImage* 35, 698–708. doi: 10.1016/j.neuroimage.2006.12.027.

Zeuzem, S., Olbrich, H. G., Seeger, C., Kober, G., Schöffling, K., and Caspary, W. F. (1991). Beat-to-beat variation of heart rate in diabetic patients with autonomic neuropathy and in completely cardiac denervated patients following orthotopic heart transplantation. *Int. J. Cardiol.* 33, 105–114. doi: 10.1016/0167-5273(91)90158-L.

Ziegler, G., Dahnke, R., Yeragani, V. K., and Bär, K.-J. (2009). The relation of ventromedial prefrontal cortex activity and heart rate fluctuations at rest. *Eur. J. Neurosci.* 30, 2205–2210. doi: 10.1111/j.1460-9568.2009.07008.x.

This is a provisional file, not the final typeset article

Figures

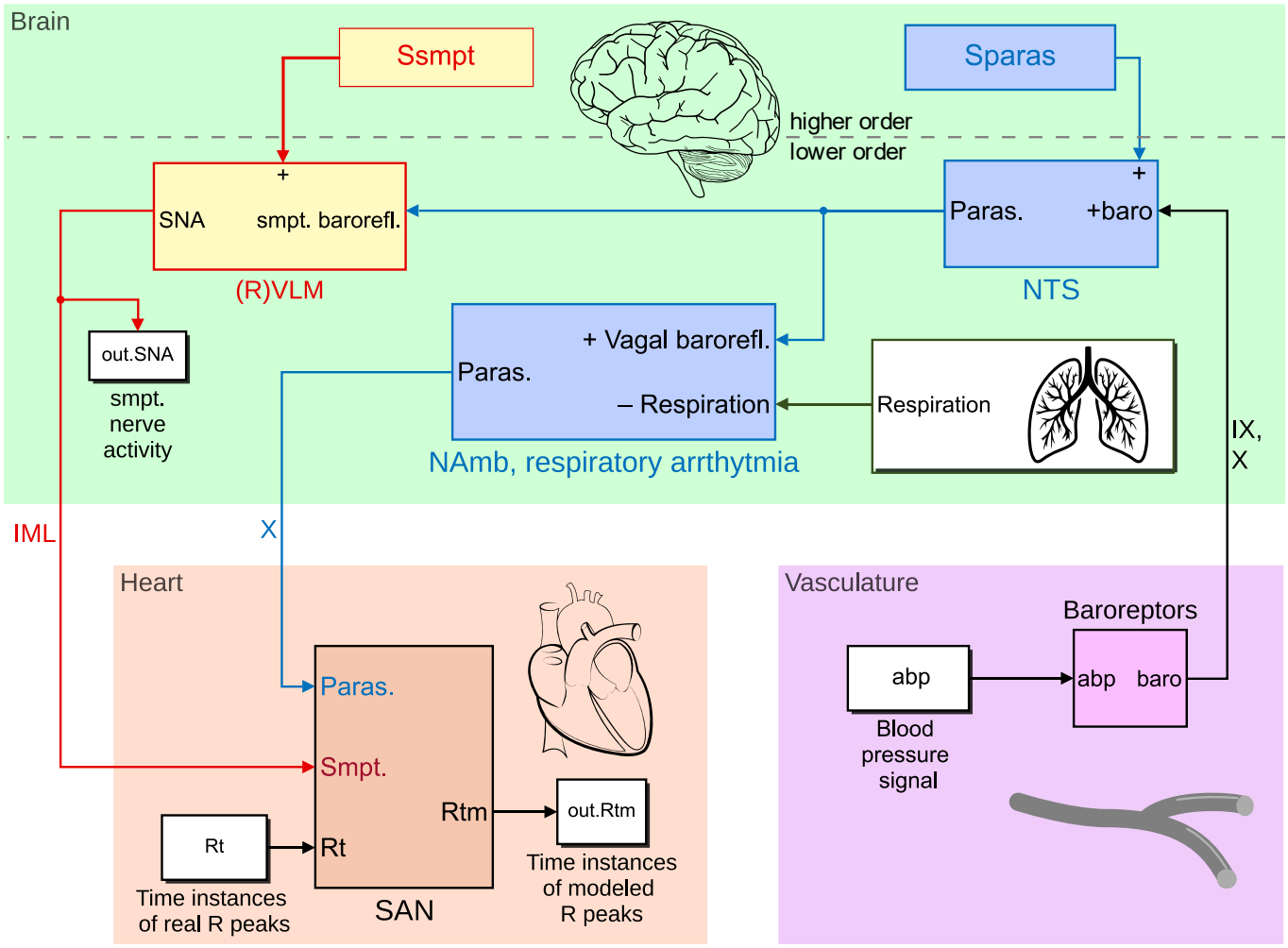

Figure 1. Heart rate regulation model overview scheme in Simulink. It encompasses three main domains: 1) heart (orange), 2) brain (green) – higher-order neural control, also lower-order neural control via respiratory sinus arrhythmia and baroreflex, and 3) vasculature (pink). Abbreviations of structures: IML, intermediolateral column; IX, nervus glossopharyngeus; NAmb, nucleus ambiguus; NTS, nucleus tractus solitarius; (R)VLM, (rostral) ventrolateral medulla; SAN, sinoatrial node; X, nervus vagus. Other abbreviations: baro, activity of baroafferents; paras, parasympathetic activity; smpt, sympathetic activity; Sparas, higher-order parasympathetic activity; Ssmpt, higher-order sympathetic activity; out – output variable. Most modules of this general scheme have more detailed internal algorithmic structure described in dedicated sub-chapter.

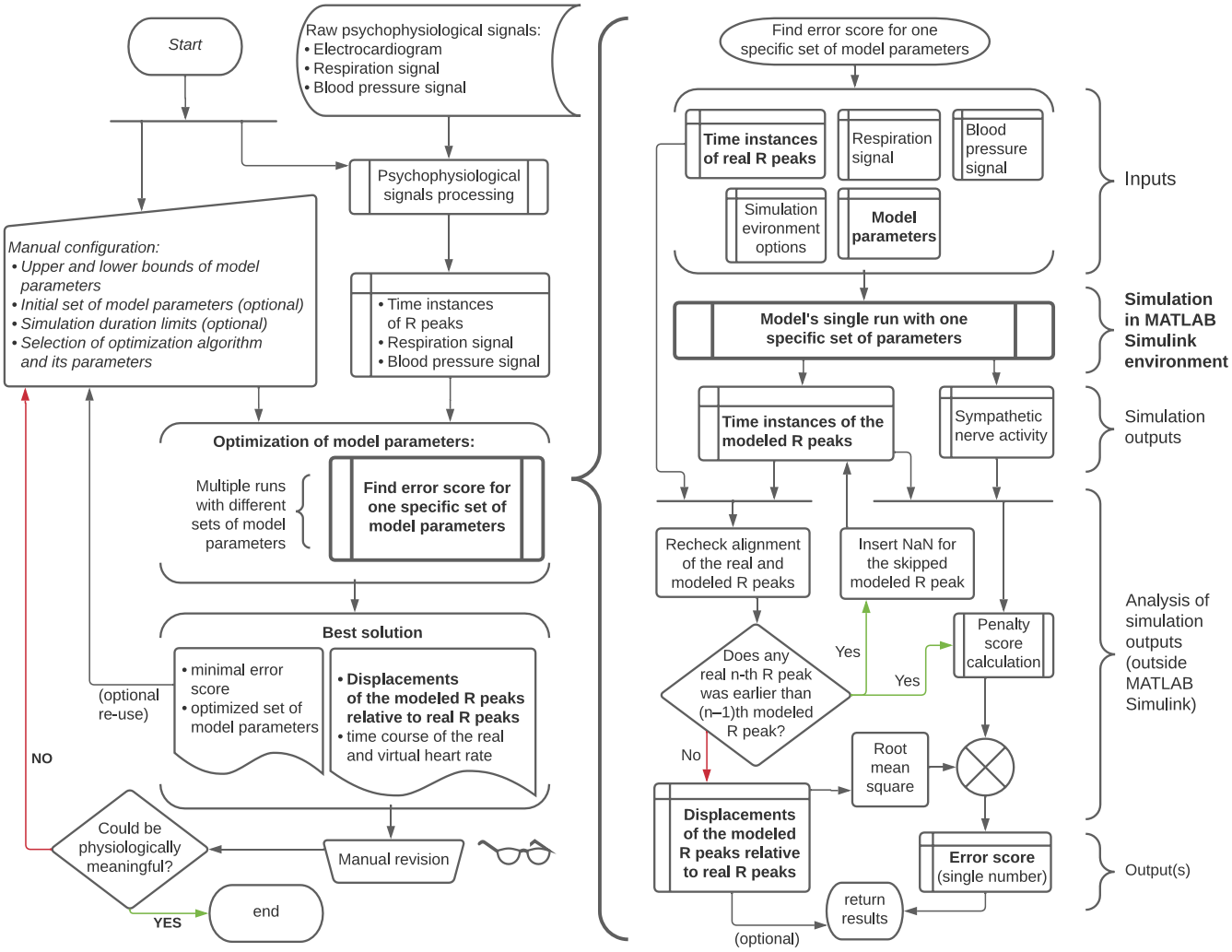

Figure 2. Algorithmic scheme of concept. Here "model" (and "Model's single run with one specific set of parameters") refers to heart rate regulation model realized in MATLAB Simulink environment. Although this model usually returns the modeled R peaks aligned to the real ones, re-check and correction is needed for rare cases of the skipped modeled R peak(s). NaN – not a number.

This is a provisional file, not the final typeset article

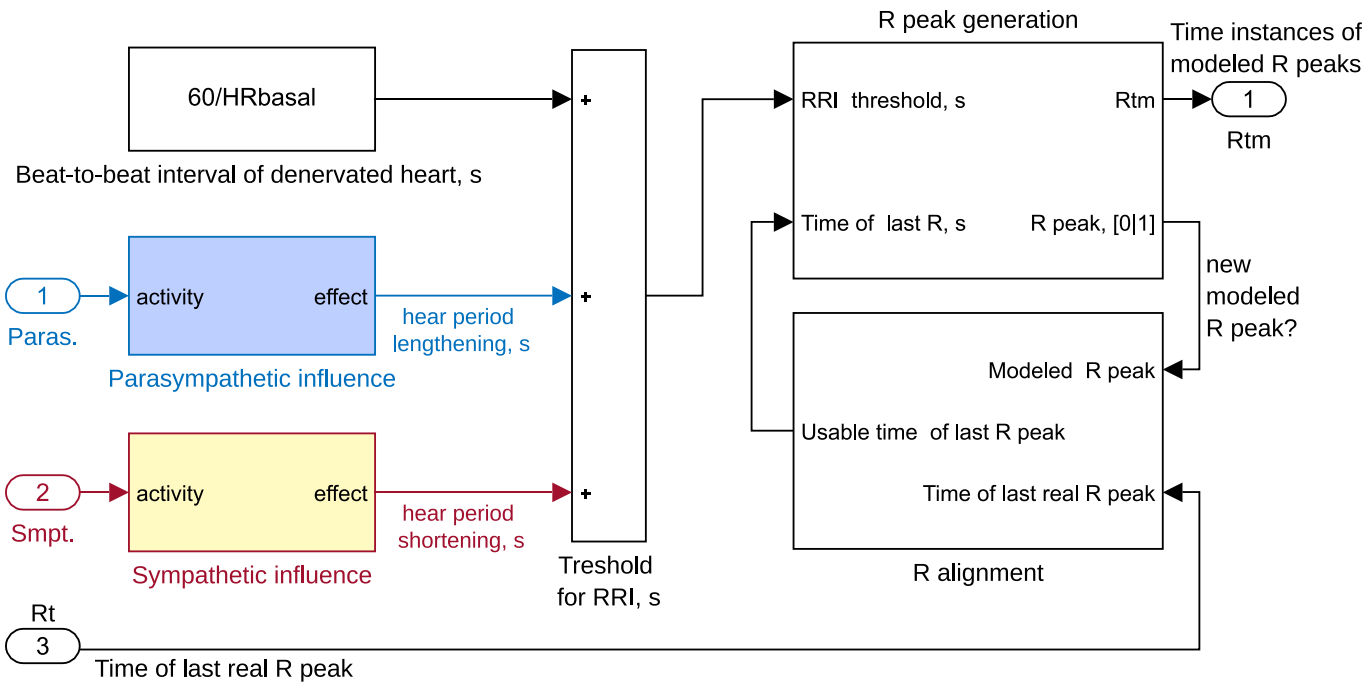

Figure 3. Sinoatrial node block scheme in Simulink. Two switches can be optionally used: switch on for real time instances of last R peak – to align real and model R peaks and find out lack or surplus of threshold for each R peak time during analysis outside the model; another switch is for R peak selection – real or modeled – to be passed for cardiac output generation in left ventricle – to control influences on arterial pressure. RRI – R-R intervals; *HRbasal* – pacemaker's internal frequency.

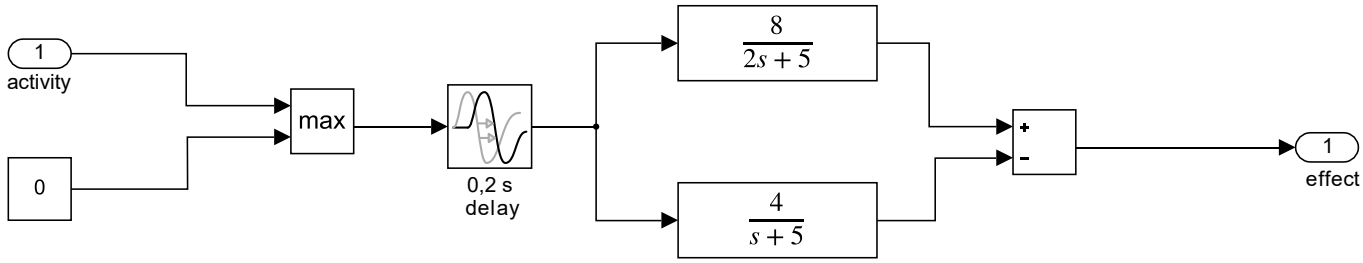

Figure 4. Parasympathetic influence sub-block of sinoatrial node block in Simulink.

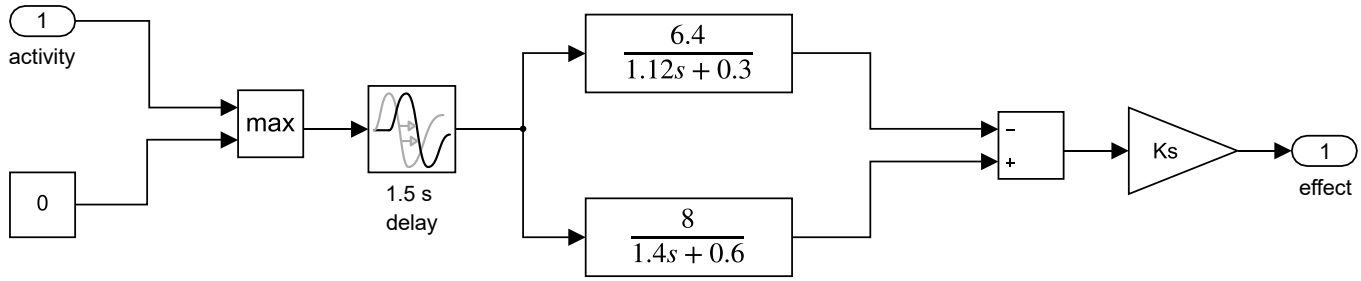

Figure 5. Sympathetic influence sub-block of sinoatrial node block in Simulink.

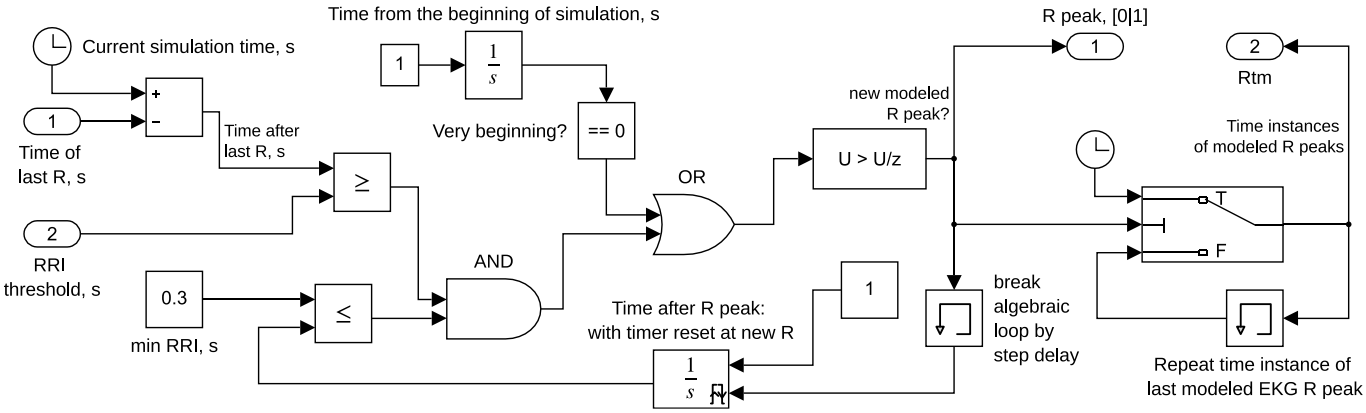

Figure 6. EKG R peak generation sub-block in Simulink. When the accumulated time after the last R peak is more than 300 ms and hits the dynamically changing RRI threshold, the pacemaker fires (new R peak is generated) and is immediately reset to zero. Note 1: "current simulation time" and "time from the beginning of simulation" will not be the same if simulation starts not at zero second of psychophysiological recording. Note 2: modeled R time instances may be not the same as "time of last R" if R alignment is enabled outside this sub-block. Time instances of modeled R peaks are stored in memory (here "out.Rtm") for analysis outside model.

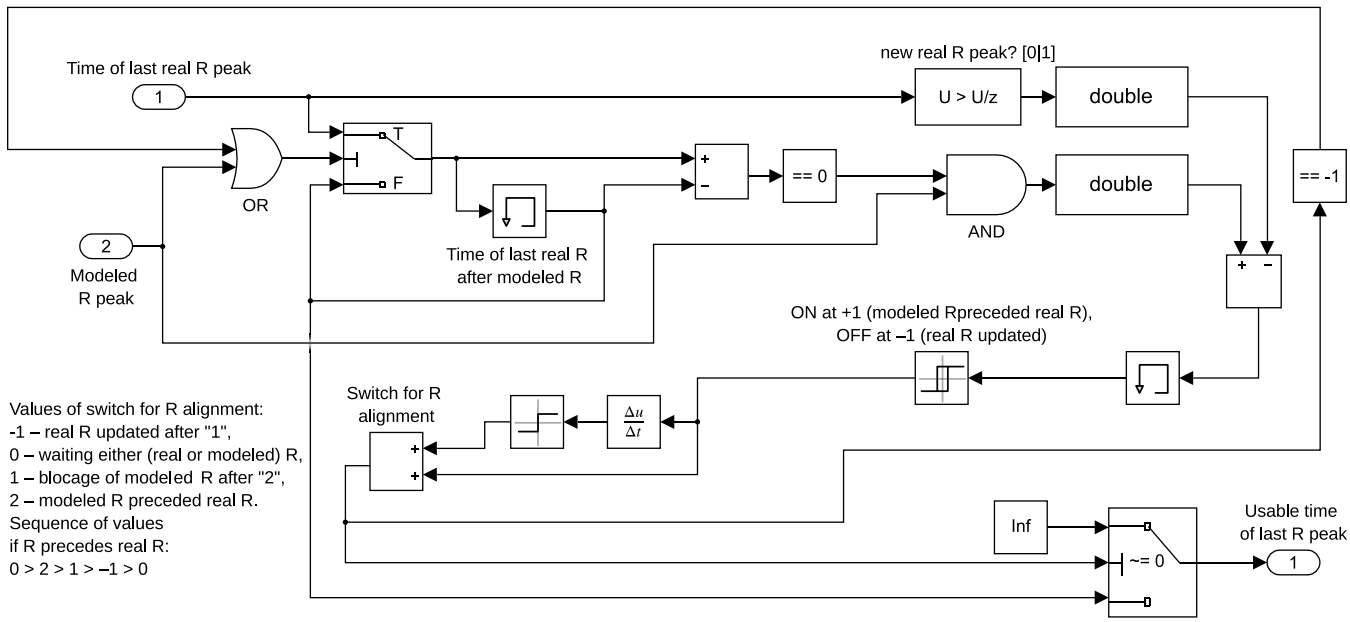

Figure 7. Simulink sub-block for alignment of the real and modeled R peaks.

This is a provisional file, not the final typeset article

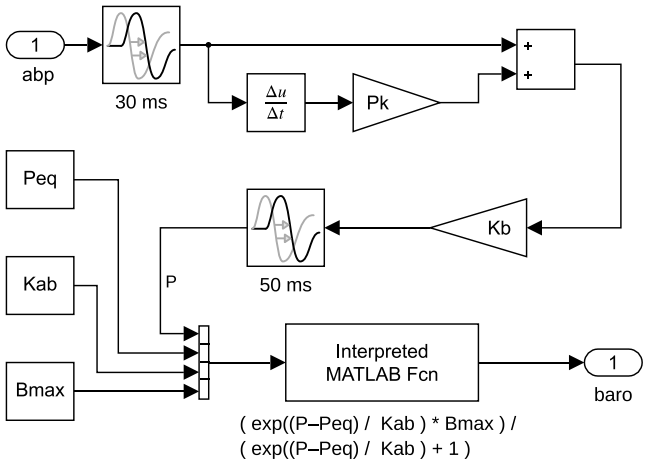

Figure 8. Simulation of integrated baroreceptors responses (baro) from arterial blood pressure (abp) signal in Simulink.

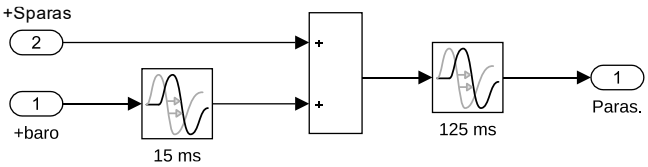

Figure 9. Nucleus tractus solitarius scheme in Simulink.

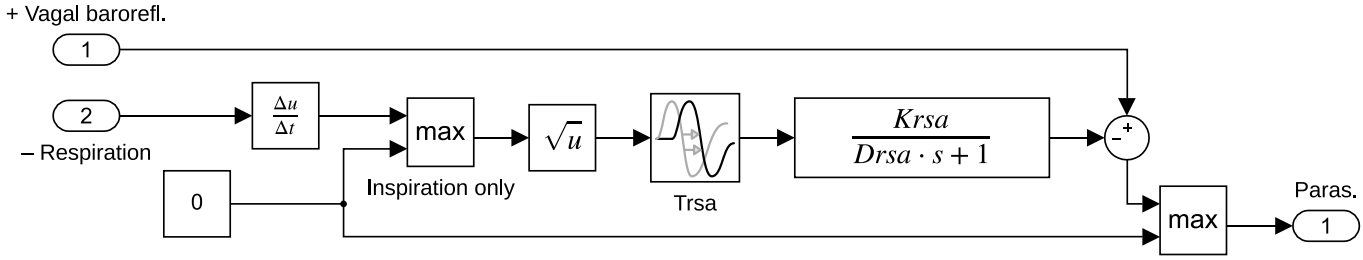

Figure 10. Nucleus ambiguus scheme for **respiratory arrhythmia** in Simulink: parasympathetic activity ('Vagal baroreflex' input #1) is inhibited during inspiration with little time delay *Trsa*. Inhibition strength depends on respiration (input #2) signal derivative (its square root), transfer function (where *Drsa* is in denominator) and custom *Krsa* coefficient.

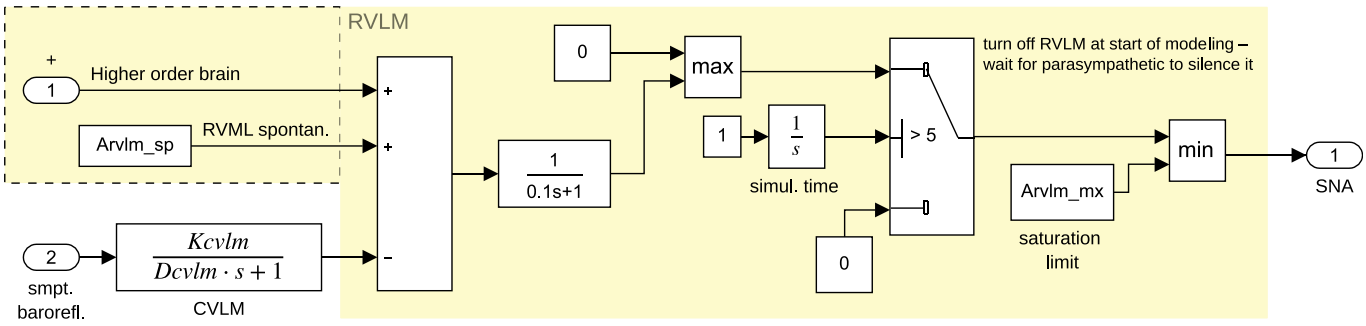

Figure 11. Rostral ventrolateral medulla (RVLM) algorithmic structure in Simulink to generate pulsatile sympathetic nerve activity (SNA) when it is not fully blocked by caudal ventrolateral medulla (CVLM). Variables: *Arvlm_sp* – constant spontaneous RVLM internal activity, *Arvlm_mx* – saturation limit of RVML output; *Dcvml* and *Kcvml* – NTS parasympathetic effect on sympathetic activity coefficient.

This is a provisional file, not the final typeset article

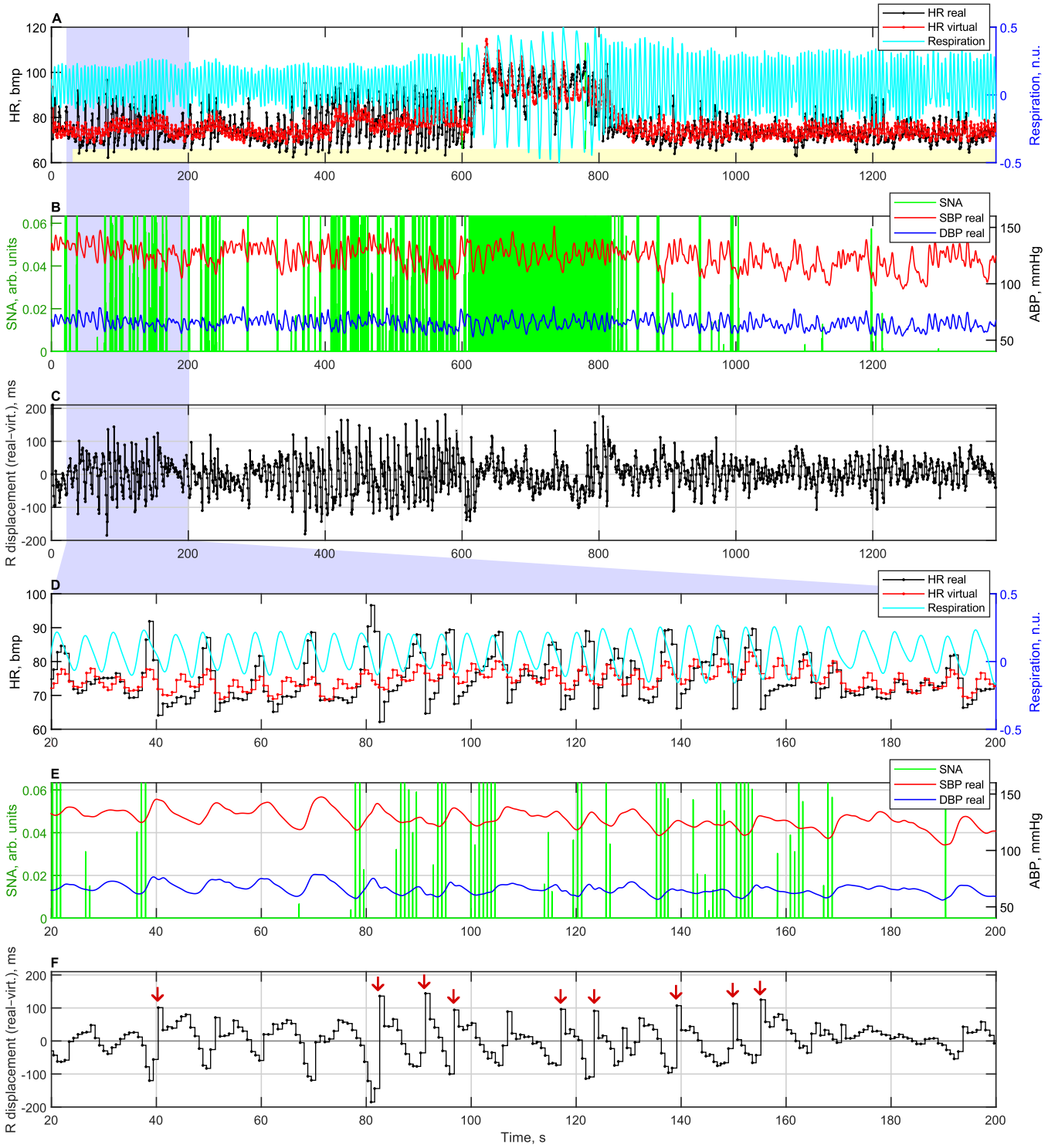

Figure 12. Psychophysiological data of a 33-year-old male: time course of the real and virtual heart rate (HR), respiration (A and D parts), the modeled sympathetic nerve activity (SNA) and the processed real arterial blood pressure (ABP) (B and E parts), R peak displacements (C and F parts). A, B, and C parts are zoomed in D, E, and F. Slow respiration condition period was from 600 to 780 second (green dashed marks in A part); other periods are resting state. HR model calibrated for period from 30 to 1380 second (light yellow strip at bottom of A part). Other abbreviations: DBP, diastolic blood pressure; SBP, systolic blood pressure.

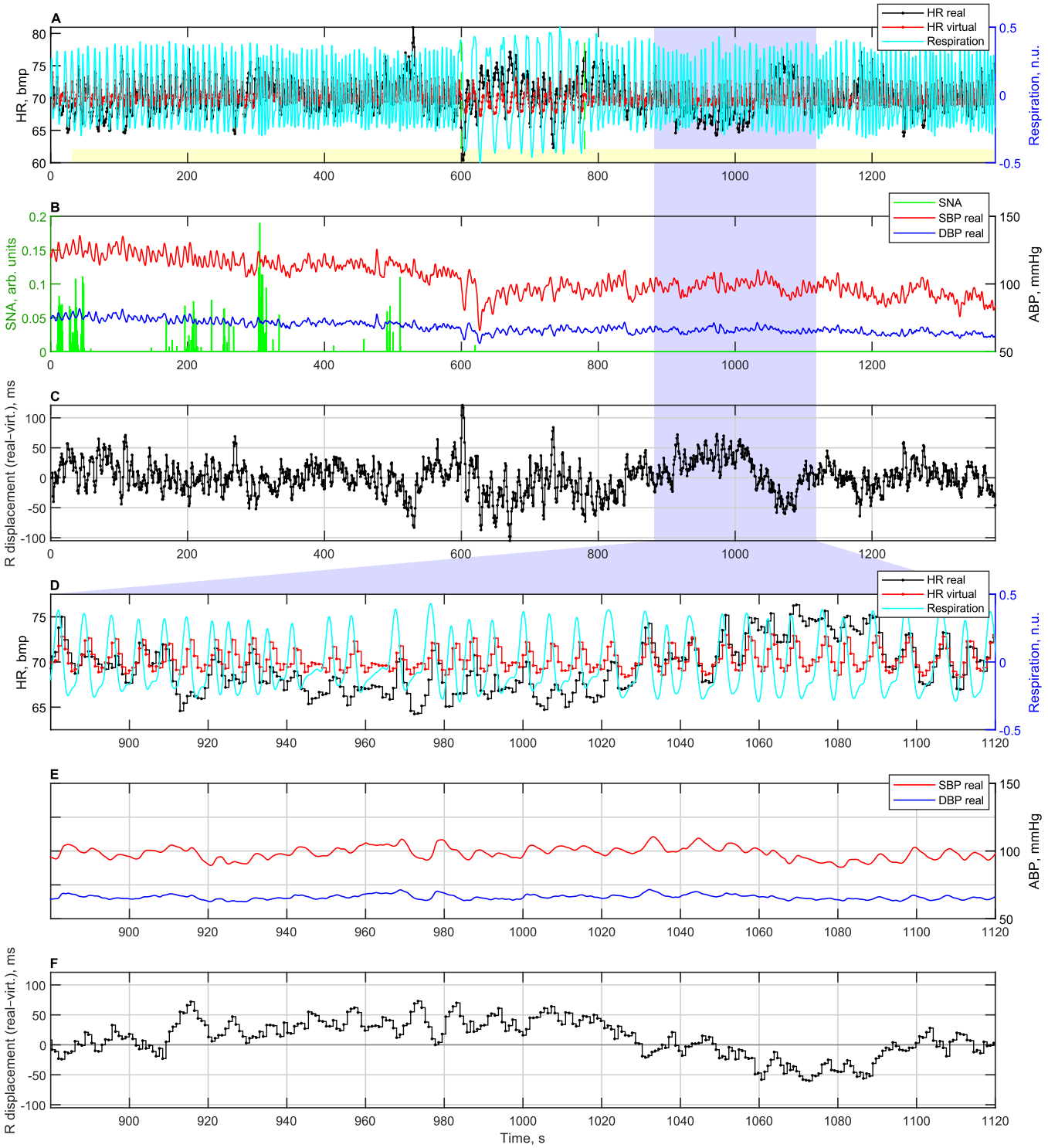

Figure 13. Psychophysiological data of a 50-year-old male: time course of the real and virtual heart rate (HR), respiration (A and D parts), the modeled sympathetic nerve activity (SNA) and the processed real arterial blood pressure (ABP) (B and E parts), R peak displacements (C and F parts). A, B, and C parts are zoomed in D, E, and F. Slow respiration condition period was from 600 to 780 second (green dashed marks in A part); other periods are resting state. HR model calibrated for period from 30 to 1380 second (light yellow strip at bottom of A part). Other abbreviations: DBP, diastolic blood pressure; SBP, systolic blood pressure.

This is a provisional file, not the final typeset article

Tables

Table 1. Summary of the personalizable heart rate regulation model parameters. Abbreviations: ABP, arterial (blood) pressure; CVLM, caudal ventrolateral medulla; NAmb, nucleus ambiguus; NTS, nucleus tractus solitarius; RSA, respiratory sinus arrhythmia; (R)VLM, (rostral) ventrolateral medulla; SAN, sinoatrial node.

Mechanisms: Domain	Parameter name	Range for optimization	Personalized value		Units	Description
			33y subj.	50y subj.		
All: Brain	Sparas	[0 1]	0.014605	0.116169	–	Brain parasympathetic basal level
All: Heart/SAN	HRbasal	[70 120]	107.6261	83.02557	beats/min	Rate of denervated heart at SAN.
RSA: Brain/NAmb	Drsa	[0.4 2.5]	0.767133	1.226438	–	Transfer function denominator at NAmb for RSA
	Krsa	[0 2]	0.250125	0.182839	–	RSA coefficient at NAmb
	Trsa	[0 1]	0.544354	0.540044	s	Time delay between respiration signal and RSA effect
Sympathetic baroreflex: Brain	Ssmpt	0	0	0	–	Theoretically brain sympathetic basal level, practically merged with *Arvlm_sp* and thus here set to 0
Sympathetic baroreflex: Brain/(R)VLM	Arvlm_sp	[0 5]	1.692973	4.651536	–	Theoretically only constant spontaneous RVLM internal activity, practically brain sympathetic basal level is added
	Arvlm_mx	[0.001 0.5]	0.063362	0.456075	–	Saturation limit of RVML output
	Kcvlm	[0 30]	6.644312	27.55722	–	NTS parasympathetic effect on sympathetic activity coefficient at CVLM
	Dcvlm	[0.1 1]	0.100638	0.10884	–	Transfer function denominator at CVLM
Sympathetic baroreflex: Heart/SAN	Ks	[0 10]	1.952591	0.272138	–	Sympathetic activity coefficient at SAN
Vagal and sympathetic baroreflexes: Vasculature/ Baroreceptors	Pk	[0 5]	0.30804	0.888058	–	ABP derivative coefficient for baroreception
	Kb	[0.01 10]	2.302123	2.749199	–	Scaling factor of ABP and its derivative sum for baroreception
	Peq	[80 100]	89.19561	82.82140	mmHg	Central point of the sigmoidal functional for baroreception
	Kab	[1 50]	17.72824	16.47293	–	Slope-related coefficient for baroreception
	Bmax	[0 5]	0.450024	0.107924	–	Baroafferent activity saturation level